Materials Science for Energy Technologies 3 (2020) 853–861

Contents lists available at ScienceDirect

Materials Science for Energy Technologies

journal homepage: www.keaipublishing.com/en/journals/materials-science-for-energy-technologies

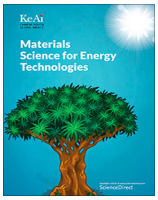

Photocatalytic, antibacterial and electrochemical properties of novel rare earth metal oxides-based nanohybrids

Karthik Kannan [a], D. Radhika [b,*], A.S Nesaraj [c], Kishor Kumar Sadasivuni [a], Kakarla Raghava Reddy [d], Deepak Kasai [b], Anjanapura V. Raghu [b,*]

[a] Center for Advanced Materials, Qatar University, P.O Box 2713, Qatar
[b] Department of Chemistry, Faculty of Engineering and Technology, Jain-Deemed to be University, Jakkasandra, Ramnagara 562112, Karnataka, India
[c] Department of Chemistry, Karunya Institute of Technology and Sciences, Coimbatore – 641 114, Tamil Nadu, India
[d] School of Chemical and Biomolecular Engineering, The University of Sydney, NSW 2006, Australia

ARTICLE INFO

Article history:
Received 9 September 2020
Revised 28 October 2020
Accepted 28 October 2020
Available online 8 November 2020

Keywords:
NiO nanohybrids
NiO-CGSO
Photocatalysis
Energy storage devices
Photocatalytic activity
Antibacterial activity

ABSTRACT

Mixed metal oxide nanocomposites (rare earth-based) have become irreplaceable and tend to display great functioning in all kinds of arenas like as photocatalytic, electrochemical, and biological. NiO-CGSO [NiO-$Ce_{0.8}Gd_{0.2}O_{2-\delta}$–$Ce_{0.8}Sm_{0.2}O_{2-\delta}$] nanomaterial was produced by the wet-chemical route for numerous purposes. The development of (FCC) face-centered cubic structure confirmed and there was no derivative phase was observed by XRD. Metal-Oxygen bond was revealed by FTIR analysis. The morphology and elemental composition of the sample were carried out using SEM with EDAX. The optical bandgap of prepared nanocomposite was studied using UV–Vis spectroscopy. Electrochemical behaviour was observed at conditions, voltage (1.3 V), and the frequency (42 Hz–5 kHz). Photocatalytic and antibacterial behavior of prepared NiO-CGSO nanocomposites also investigated. It was found that this novel composite catalyst decomposed 92% of toxic pollutants from wastewater. Further, NiO-CGSO composites showed superior antibacterial performance against *aeromonas hydrophila*, *E. coli*, and *S. epidermis* bacterial pathogens.

1. Introduction

Metal oxide nanocomposites (NCs) have extensive appliances for instance photocatalysis, chemical, biosensors, and anti-resistant bacteria and therapeutic agents [1]. In the value of ecological remediation, metal oxide based composites have broad and develop into competent material on account of their lesser bandgap, inexpensive, non-toxicity, thermal, and chemical stability [2]. Rare-earth doped composites were intentioned as feasible anodes for IT-SOFCs. They display typical assorted electronic-ionic conductivity [3,4]. It was originated to facilitate composites that could demonstrate exceptional high electron-transfer, conduction, and noxious dyes degradation properties, consecutively, which could sustain to achieve superior power output [5–8].

From literature, it can realize that several organic and inorganic nanoparticles including CuO, NiO, MgO, CeO_2, NiO have been widely utilized in biomedical and other purposes [9–12]. Nanomaterials attracted many young scientists as a result of their appreciable chemical stability, magnetic behaviour, and biocompatibility. The nanomaterials are also eminent in the antibacterial, antifungal, antioxidant, and anticancer activities [13,14].

In the meantime, the photocatalytic semiconductor has prompted scientific awareness owing to their prevalent purposes for the decrease of infectivity from the water and air. It is mostly utilized for H_2 production, odor control, and stimulation of bacteria and tumor cells. The pollutants released straight to the atmosphere need to be photo degraded not including the creation of added misuse and byproducts into H_2O and carbon dioxide [15]. It is an eminent authenticity that water effluence is an enormous confront for the existing and forthcoming generations. In the framework, dyes participate decisive function in the effluence of water bodies and are extremely noxious, which is frequently developed in several manufactories. As dyes show a composite structure, it is compli-

* Corresponding authors.
E-mail addresses: radhikadv8@gmail.com (D. Radhika), gsraghu2003@yahoo.co.in (A.V. Raghu).

Peer review under responsibility of KeAi Communications Co., Ltd.

https://doi.org/10.1016/j.mset.2020.10.008

cated to humiliate in nature. As a result, diverse semiconductor photocatalysis procedures have been implemented to humiliate the unrefined pollution integrated into the water resources [16]. Among many metal oxide nanoparticles (NPs), NiO NPs are widely applied on account of their large bandgap, chemical stability, non-toxicity, and electrochemical activity [8,17]**.** Such impending properties correlated with the NiO NPs in dissimilar fields like therapeutic, magnetic hyperthermia, sensing, and other applications [9,17–19].

Different techniques have been executed for nanocomposites (NCs) production such as ultra-sonic process, ball milling, microwave, mechanical alloying, sol–gel and chemical-precipitation, etc [21–23]. From above all well-framed methods, the co-precipitation technique is utilized as a valuable scheme for the synthesis of nanoparticles, due to a pleasant route. It targets a swift and harmonized method of reaction as an alternative of formulating from exterior resources. This technique is extra operative for capitulating homogeneity, awfully untainted model, miniature particle size, lesser time, and less exterior energy [25–28]. In this current work, Gd and Sm doped ceria material was inspected methodically using C-TAB surfactant. Cerium has so many applications and especially involved in catalysis and shown excellent features as reported earlier [29]. Also, rare-earth nanostructures have various applications as reported by many researchers [31–35].

In the present work, for the first time, novel NiO-CGSO nanohybrids were synthesized using a wet chemical method in the presence of CTAB surfactant. Synthesized nanohybrids were investigated to determine structural, morphological, antibacterial and electrochemical performance. Further, the study is broadened to inspect the removal of toxic pollutants through the photocatalytic process.

2. Experimental method

2.1. Materials

In this experimental study (NiO-CGSO NC), the aqueous solutions prepared and materials as similar to our earlier report [37,37].

2.2. Method

The flowchart of the procedure for the fabrication of NiO-CGSO NC is revealed in Fig. 1.

2.3. Reactions involved in mechanism: Stepwise

Step by step reactions entailed in the fabrication of NiO-CGSO NC during the experiment can be shown below:

Reaction mechanism for NiO-CGSO

(i) $7.6NaOH \xrightarrow{H_2O} 7.6Na^{+}_{(aq)} + 7.6OH^{-}_{(aq)}$

(ii) $Ni(NO_3)_2 \xrightarrow{H_2O} Ni^{2+}_{(aq)} + 2NO_3{}^{-}_{(aq)}$

(iii) $1.6Ce(NO_3)_3.6H_2O_{(aq)} \xrightarrow{H_2O} 1.6Ce^{3+}_{(aq)} + 4.8NO_3{}^{-}_{(aq)} + 6H_2O_{(aq)}$

(iv) $0.2Gd(NO_3)_3 \xrightarrow{H_2O} 0.2Gd^{3+}_{(aq)} + 0.6NO_3{}^{-}_{(aq)}$

(v) $0.2Sm(NO_3)_3 \xrightarrow{H_2O} 0.2Sm^{3+}_{(aq)} + 0.6NO_3{}^{-}_{(aq)}$

(vi) $1.6Ce^{3+}_{(aq)} + Ni^{2+}_{(aq)} + 0.2Gd^{3+}_{(aq)} + 0.2Sm^{3+}_{(aq)} + 7.6OH^{-}_{(aq)} + xH_2O_{(aq)} \xrightarrow{stirring} 1.6Ce(OH)_4.xH_2O_{(s)} \downarrow + Ni(OH)_2.xH_2O_{(s)} \downarrow + 0.2Gd(OH)_3.xH_2O_{(s)} \downarrow + 0.2Sm(OH)_3.xH_2O_{(s)} \downarrow$

(vii) $1.6Ce(OH)_4.xH_2O_{(s)} + Ni(OH)_2.xH_2O_{(s)} + 0.2Gd(OH)_3.xH_2O_{(s)} + 0.2Sm(OH)_3.xH_2O_{(s)} \xrightarrow{500-100^{\circ}C} 1.6Ce(OH)_4 + Ni(OH)_2 + 0.2Gd(OH)_3 + 0.2Sm(OH)_3 + xH_2O_{(g)} \uparrow$

(viii) $1.6Ce(OH)_4 + Ni(OH)_2 + 0.2Gd(OH)_3 + 0.2Sm(OH)_3 \times \xrightarrow{300,450,600 \text{and} 750^{\circ}C} NiO - Ce_{0.8}Gd_{0.2}O_{2-\delta} - Ce_{0.8}Sm_{0.2}O_{2-\delta(s)} + xH_2O_{(g)} \uparrow$

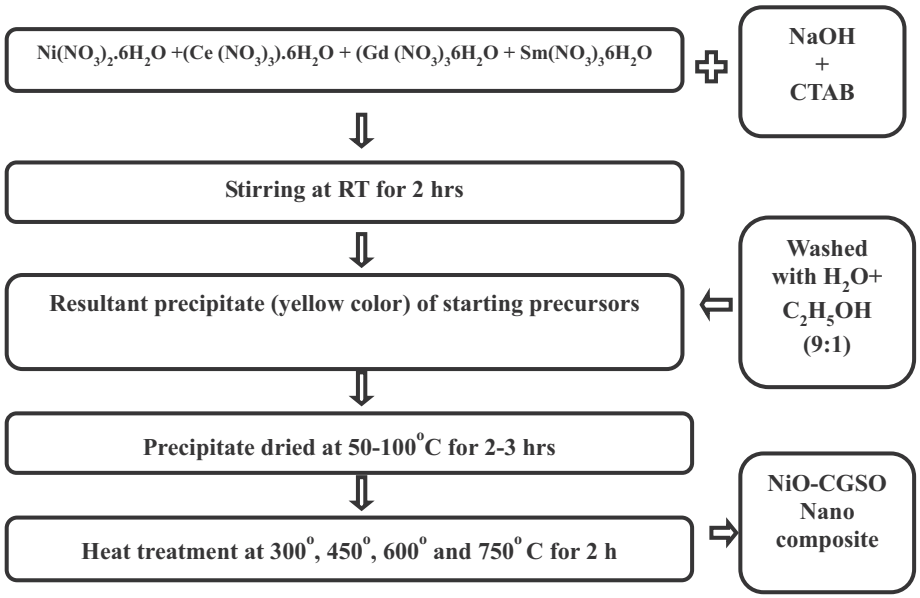

Fig. 1. Flowchart of NiO-CGSO NC preparation.

Overall balanced equation:

$$7.6NaOH + 1.6Ce(NO_3)_3.6H_2O_{(aq)} + Ni(NO_3)_2 + 0.2Gd(NO_3)_3 + 0.2Sm(NO_3)_3 \xrightarrow{H_2O} NiO - Ce_{0.8}Gd_{0.2}O_{2-\delta} - Ce_{0.8}Sm_{0.2}O_{2-\delta(s)} + 7.6NaNO_3(aq) + xH_2O_{(g)} \uparrow$$

2.4. Characterization

To characterize the synthesized composite powders, the phase of the samples was investigated by XRD operating the Shimadzu XRD 6000 X-ray diffractometer K_α radiations (λ = 1.5418 Å). FTIR spectra were recorded using the JASCO 460 Plus spectrometer over the range from 4000 to 400 cm^{-1}. For this analysis, a small amount of Y_2O_3 samples was blended with KBr and then pressed into pellets for the measurement. The changes in surface morphology of the products were monitored by a scanning electron microscopy (JEOL Model JSM-6360 SEM) operated at 15 kV. Thermal behavior was examined on a Perkin Elmer TGA 7 under N_2 atmosphere at 10 °C/min of heating rate. The UV–vis absorption spectrum was obtained from the Agilent 8453 diode array UV–Vis spectrophotometer. The bulk conductivity was projected via impedance analysis. The photocatalytic behavior of the composite was studied under natural light irradiation, and the antimicrobial behavior of the composite was studied by the agar well diffusion method.

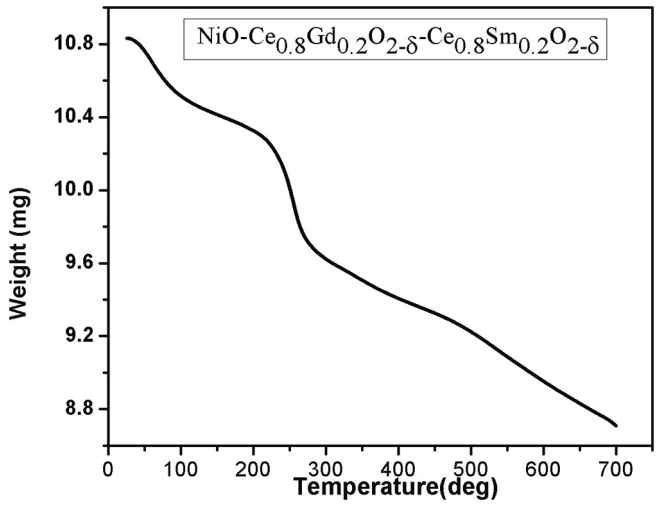

Fig. 2. TGA pattern of the precursor material.

Table 1
Weight loss regions of the forerunner material.

Phase/ Region	Temperature (°C)	Weight failure	Explanation
I	100	1–2%	Water molecule thrashing
II	250	5–6%	Phase arrangement of NiO
III	Among 250 to 700	Over 6%	carbon/nitrogen-based compounds decomposition
IV	Approximately 700	Steadiness in Weight loss	Phase-pure nanocomposite configuration

3. Results and discussion

3.1. Thermal properties

The prepared forerunner material (Hydroxides of Ni, Ce, Gd, and Sm) by a prelude mass of 8–12 mg was positioned (Pt crucible) and proceed for examination and the output was shown in Fig. 2.

From the above curve, it was assumed that the loss of weight starts to show from the earlier phase itself. The NC thermal decomposition can be allocated into 4 split sections as explained in the earlier reports [5,38] and also the loss of weight modification detected for the forerunner material attained from the TGA data displayed in Tables 1 and 2 respectively.

3.2. Morphological and structural studies

3.2.1. Crystallinity

The XRD of the NiO-CGSO NC discloses the design of FCC (fluorite cubic) well crystalline single-phase as shown in Fig. 3 [40–41]. There are no contamination peaks or any other secondary phase was examined in the XRD pattern of NiO-CGSO NC and the crystallographic planes viewed at (1 1 1), (2 0 0), (2 2 0), (3 1 1), (2 2 2), (4 0 0), (3 3 1), (4 2 0) and (4 2 2) as per JCPDS No: 81-0792 are designated in CeO_2 phase [42]. The crystallographic planes observed at (1 1 1), (2 0 0) and (2 2 0) as per JCPDS No: 75-0197 are designated in the NiO phase [43].

The structural parameters of the samples were computed (from the XRD data) as reported earlier [20,25,44] and the obtained values shown in Table 3.

3.2.2. FTIR studies

FTIR spectrum of NIO-CGSO NC was exposed in Fig. 4. The significant peaks noticed from the FTIR spectrum ascribed for distinguishing peaks have been listed in Table 4.

3.2.3. Morphological studies

The SEM characterization and EDAX analysis of images acquired on NiO-CGSO NC calcined at 750 °C are presented in Fig. 5. SEM

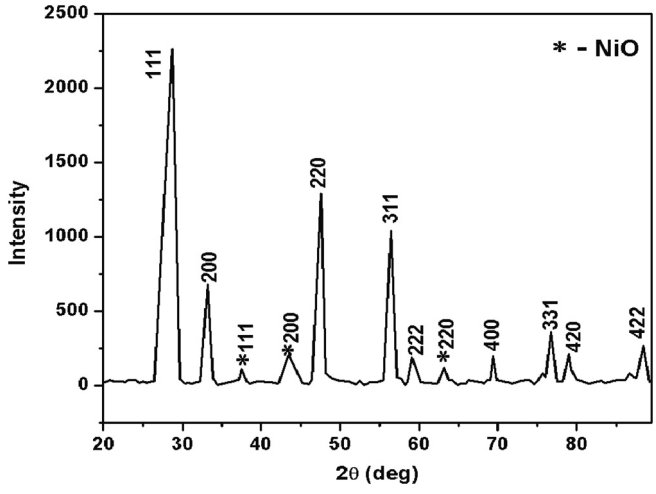

Fig. 3. The obtained XRD pattern of NiO-CGSO NC.

Table 2
Change in weight reduction recorded from the TGA of precursor material.

Sample	Primary weight (mg) at 25 °C	Final weight (mg) at 700 °C	Total weight loss (mg)	Total Weight loss (%)
NiO-CGSO	10.83	8.70	2.13	22%

Table 3
The structural parameters of NiO- NC.

Lattice parameter	CeO_2 phase (JCPDS No. 81–0792)	Doped CeO_2 phase of NiO-CGSO	NiO phase (JCPDS No. 75–0792)	NiO phase of NiO-CGSO
Crystallite structure	Cubic (FCC)	Cubic (FCC)	Cubic (FCC)	Cubic (FCC)
Lattice parameter 'a' (Å)	5.412	5.412	4.170	4.161
Lattice volume ($Å^3$)	158.516	158.516	72.511	72.043
Speculative density (g/cc)	7.2110	8.139	6.8430	6.885
Crystallite size (nm)	20.8	–	20.8	–

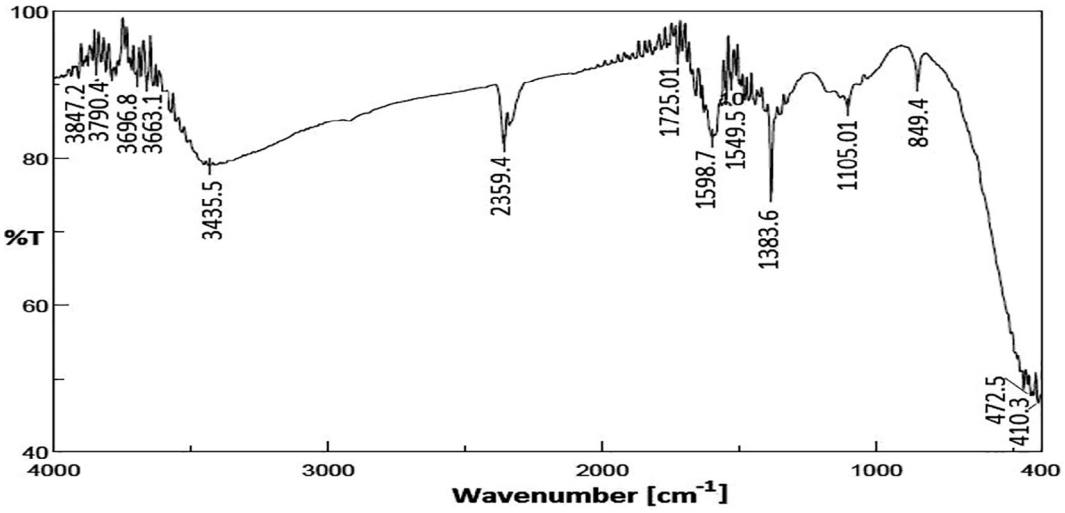

Fig. 4. FTIR spectrum obtained on NiO-CGSO NC.

Table 4
FTIR consignments of the prepared sample.

Material	Obligation of distinctive peaks (Cm^{-1})				
	Ce-O	Ni-O	Carbon dioxide	δ (H-O–H) bending	OH stretching
Reference Peaks	1383.2	Near 400	2360.5	1600.7	3400.8
NiO-CGSO	1384	410	2359	1599	3435
Ref.	[46]	[45]	[47]	[46]	[45]

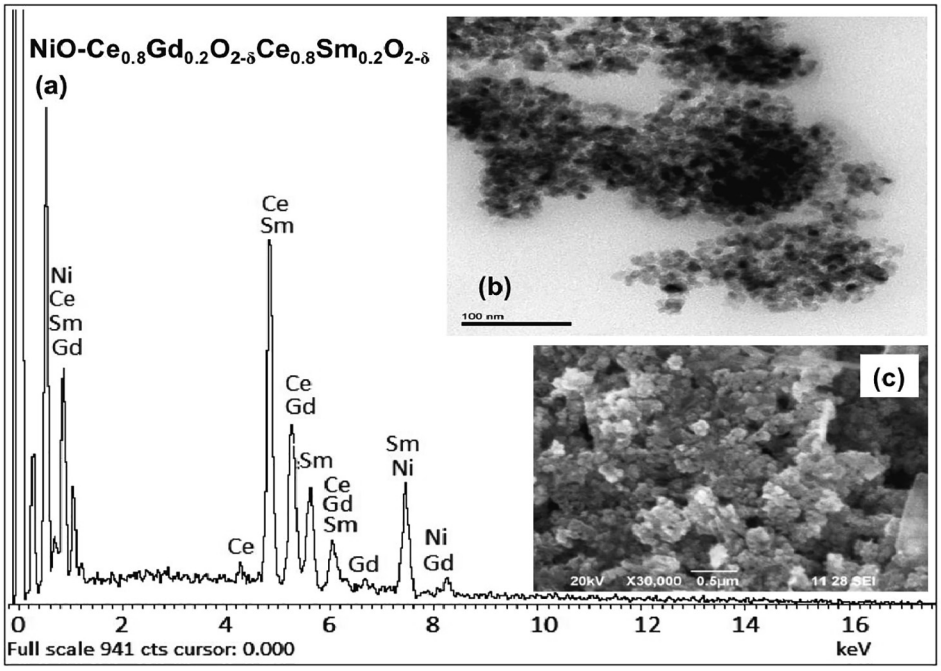

Fig. 5. (a) EDAX, (b) TEM, and (c) SEM data obtained on NiO-CGSO nanocomposite.

photographs (Fig. 5c) and TEM images (Fig. 5b) were displayed in Fig. 5.

TEM and SEM pictures obtained on NiO-CGSO NC reveal the clear spherical shaped particles and the size was shown in the range of 30 to 60 nm. It is also observed that the minority microparticles showed owing to cluster [25,25]. The supplement of the CTAB (surfactant) prohibited the chance of remarkable cluster to achieve well NC. EDAX disclosed the occurrence of the elemental composition obtained from the NiO-CGSO NC as Ni (13.4%), Ce (49.4%), Gd (5.8%), Sm (4.2%), and O (27.2%). There are no contamination peaks observed in EDAX spectra and also suggested the purity of the composite.

3.2.4. Optical studies

The optical studies of NiO-CGSO NC were deliberated by UV–Visible spectroscopy. The spectrum was recorded in the region from 200 to 800 nm wavelength at RT. The energy bandgap of the NC can be determined from the E_g measurements via tauc's relation formula. The nanocomposite exhibits a strong absorbance peak (350 nm) wavelength. The analyzed bandgap of NiO-CGSO composite was initiated to be 3.54 eV [27–28].

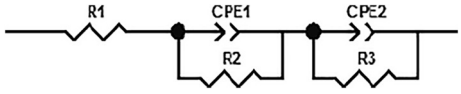

Fig. 6. Corresponding circuit (2RQR) employed for fitting data.

3.3. Electrochemical behavior

The circular compacts of prepared the NC, diameter (10 mm), thickness (2 mm), and pressure (1.2 ton) using hydraulic pressure pelletizer. To achieve a more densified state, the sintering temperature was applied at 750 °C for 3 h to diminish pours.

Table 5
The calculated conductivity values of NiO-CGSO NC at diverse temperatures.

Temperature (K)	Conductivity (S/cm)
310	7.8151×10^{-06}
573	7.3273×10^{-06}
673	1.2710×10^{-04}
773	4.3843×10^{-04}
873	1.2501×10^{-03}

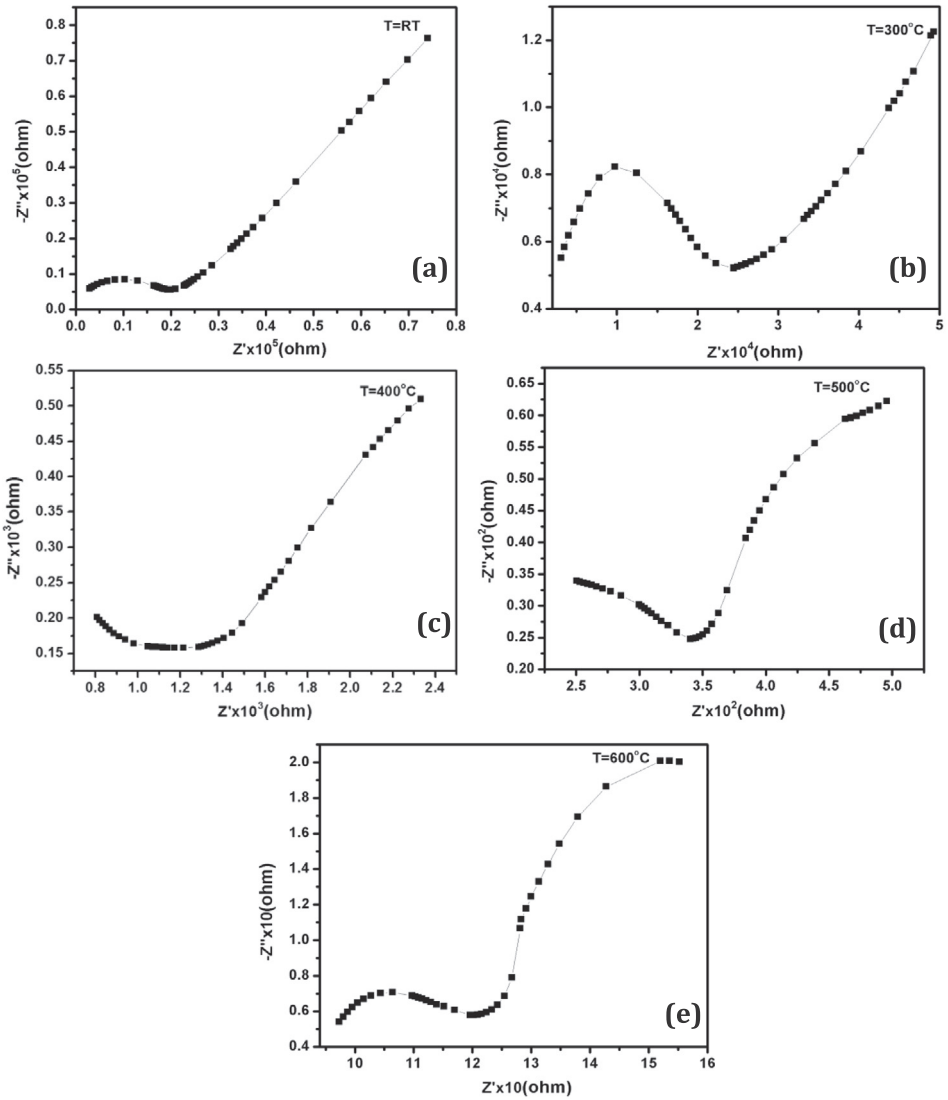

Fig. 7. (a–e) Impedance curves of NiO-CGSO NC at different temperatures.

Table 6
The calculated activation energies for NiO-CGSO NC.

Material	Temperature (°C)	1000/T (K^{-1})	logσT ($Scm^{-1}K$)	slope	Activation energy (eV)
NiO-CGSO	400	1.492	−3.895	−2.887	0.249
	500	1.298	−3.358		
	600	1.149	−2.903		

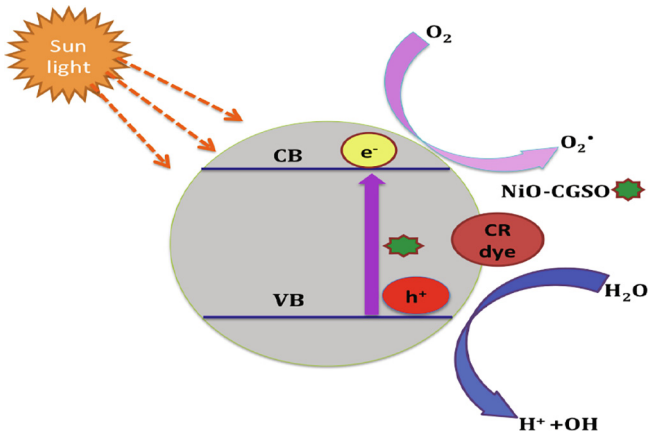

Fig. 8. Schematic mechanisms of CR dye degradation of NiO-CGSO NC.

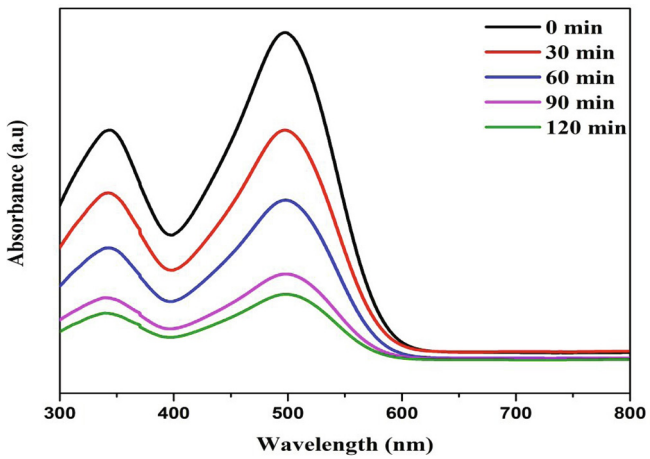

Fig. 9. Absorbance spectrum of NiO-CGSO NC for CR under nature sunlight irradiation.

At various temperatures (RT, 300, 400, 500, and 600 °C), ac impedance measurements were taken with the standard conditions. Data fitting for the measures was completed with the ZVIEW software by applying the following equivalent circuit (2RQR) and it is represented in Fig. 6. The plots obtained from the sample at diverse temperatures showed in Fig. 7(a–e).

From the data, it is observed that NiO-CGSO NC exhibited the optimum value of conductivity at high temperatures and the data shown in Table 5. Petrovsky et al reported innovative nanomaterial; Sm-doped ZrO_2 for application in ITSOFC [30–43].

The Arrhenius linear fit relationship is employed to estimate the activation energy of the prepared composite. When the conductivity enhances the activation energy also increased and the obtained values are shown in Table 6.

3.4. Photocatalytic performance

The photocatalytic nature of the NC was analyzed from the photodegradation performance of CR dye beneath the natural light irradiation process and as shown in Fig. 8. The CR degradation efficiency compared with earlier reports is shown in Table 8.

The CR dye activity of NiO-CGSO NC was evaluated under natural light irradiation. The absorption spectrum of CR is an illustration (Fig. 9) and the distinguishing absorption of CR (664 nm) diminishes hurriedly through enhanced coverage time. This specifies to facilitate the solute dye concentration declines promptly and virtually disappears in 120 min.

The degradation percentage is 92 at 120 min. The photodegradation of CR dye obeys pseudo-first-order kinetics. From the kinetics study, NiO-CGSO NC reveals an excellent CR dye action and the kinetic constant (k) is 0.0056 min^{-1}.

From Table 7, NiO-CGSO nanohybrids show importantly higher catalytic activity under natural light irradiation than the existing commercial catalyst.

3.5. Antibacterial behavior

The antimicrobial nature was assessed alongside gram-negative such as *Aeromonas hydrophila, E. coli, and S.epidermis* bacterial pathogens using NiO-CGSO NC (Fig. 10). Table 8 illustrates the Zone of inhibition (ZOI) of NiO-CGSO alongside pathogenic bacteria.

From Table 8, chemical precipitated NiO-CGSO NC show an exceptional antimicrobial activity against foodborne pathogens and also analogous with the customary antibiotics (Streptomycin).

Photolytic production of reactive oxygen species (ROS) on the surface of NiO-CGSO NC. NiO-CGSO NC is due to the formation of hydroxyl, superoxide radicals, and H_2O_2 (ROS) by the Fenton reaction leading to lipid peroxidation, DNA injure and protein decay can exterminate bacteria without destructive nonbacterial cells.

There are additional probable steps engaged in the antimicrobial activity. NiO-CGSO NC impedes the bacteria cell membrane and connects with mesosome (cellular inhalation, DNA reproduction, cell partition). These intracellular functional alterations are commenced by the oxidative stress manipulated by ROS foremost

Table 8
Antibacterial activity of NiO-CGSO NC at diverse concentrations.

Tested bacteria	Gram reaction	ZOI (mm)				Positive control (Streptomycin)	Negative control
		20 μg/mL	40 μg/mL	60 μg/mL	80 μg/mL		
S. epidermis	−ve	12	15	17	21	28	–
E. coli	−ve	14	16	19	22	25	
Aeromonas hydrophila	−ve	10	12	15	20	30	–

Table 7
Photocatalytic performance (CR dye) of NiO-CGSO NC related to metal oxide nanocomposites.

Photocatalyst	Preparation technique	Concentration	Degradation percentage (%)	Reaction time (min)	Source	Ref.
Mg-TiO_2-P25/PMS	Sonochemical	50 mg	95	120	150 W tungsten halogen lamp	[44]
Mg-TiO_2- P25/PDS			75			
Fe-$CeO_{2(P)}$	Modified auto combustion	1 g/L	87	180	100 W tungsten visible lamp	[45]
CeO_2			82			
Fe-$CeO_{2(Sg)}$			48			
$MnFe_2O_4$/ZnO	Hydrothermal	50 mg	54.4	90	Visible light	[46]
ZnO/TA/ $MnFe_2O_4$			70.2			
$MnFe_2O_4$/TA/ZnO			84.2			
g-C_3N_4/RGO/ $Bi_2Fe_4O_9$	Hydrothermal	10 mg	87.65	60	LED-30 W	[47]
$ZnMnO_3$/Fe_3O_4	Co-precipitation	0.1 g	98.17	60	5 W white LED	[48]
SnS_2-CdO	Cost-effective chemical route	6 mg	92.86	210	350 W Xenon arc lamp	[49]
Ag/1.0 Mn_3O_4	Sol-gel method	3 mg	78	120	40 W UV–Vis light irradiation	[50]
NiO-CGSO	Wet chemical route	5 mg	92	120	Sun light irradiation	Present work

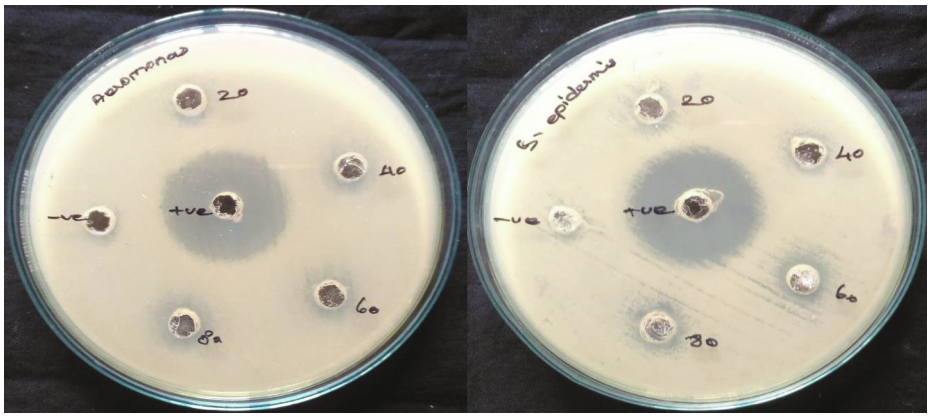

Fig. 10. Plate photos of antibacterial activity of NiO-CGSO NC.

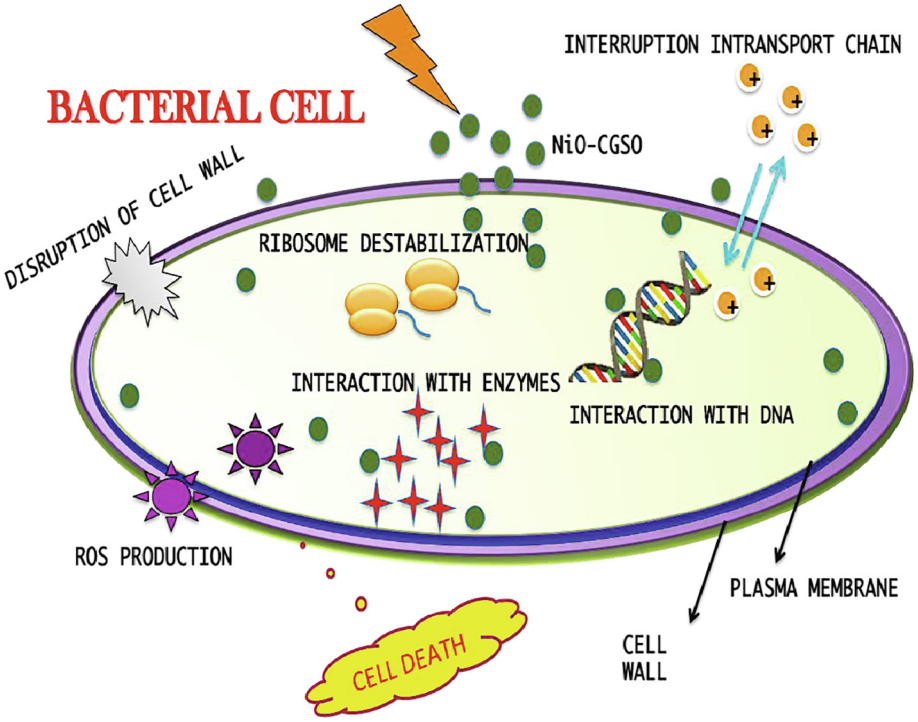

Fig. 11. Antibacterial activity mechanism of NiO-CGSO NC.

Table 9
Antibacterial activity for NiO-CGSO NC with previous reports against *E. coli.*

Materials	ZOI (mm)	Ref.
NiO.CeO_2.ZnO	11	[53]
Ag_2O.CeO_2.ZnO	12	[54]
CdO–NiO–ZnO	16	[17]
NiO-CGSO	22	Present work

to cell termination as demonstrated in Fig. 11. Only a few works of literature describe the electrostatic appeal mechanism.

Gd^{3+} and Sm^{3+} are released owing to the communication of NiO-CGSO with the microbial cell membrane. The negatively charged cell wall and positively stimulating Gd^{3+} and Sm^{3+} are mutually fascinated and they root denaturation of proteins, which outcome in thrashing of replica capacity of the DNA thus reasoning the termination of the pathogen (Table 9).

(i) $Nio - CGSO + h\upsilon \rightarrow e^- + h^+$
(ii) $h^+ + H_2O \rightarrow \cdot OH + H^+$
(iii) $e^- + O_2 \rightarrow O_2^-$
(iv) $O_2^- + H^+ \rightarrow HO_2^*$
(v) $HO_{2*} + H^+ + e^- \rightarrow H_2O_2$

The rough surface texture was responsible for mechanical injure to the cell membranes. It is comprehensible that NiO-CGSO NC has irregular crumples at the exterior surface (SEM and TEM images), which influences the antimicrobial efficacy. The higher concentrations of NiO-CGSO NC are deleterious to both the clients and microbes, but still, concentrations (nano-level) are appropriate for the annihilation of microbes [55,52].

4. Conclusion

In this work, NiO-CGSO NC was effectively extended via a wet chemical route, i.e., co-precipitation route. TGA and XRD patterns exposed the methodology to obtain phase pure materials. The prepared composite structure was validated via XRD and FTIR analysis. Using SEM and EDAX, morphology, and elemental analysis of the sample were examined. The conductivity data of the sample exposed that the sample projected in this paper might be appropriate for anode appliance in SOFC systems. The antibacterial and photocatalytic performance of prepared nanocomposite was investigated and it has shown excellent results, which are further useful to apply in different fields.

CRediT authorship contribution statement

Karthik Kannan: Conceptualization, Methodology, Writing - original draft. **D. Radhika:** Resources, Writing – review & editing, Investigation. **Kishor Kumar Sadasivuni:** Data curation. **Kakarla Raghava Reddy:** Writing – review & editing. **Deepak Kasai:** Methodology. **Anjanapura V. Raghu:** Project administration, Supervision, Writing - review & editing.

Declaration of Competing Interest

The authors declare that they have no known competing financial interests or personal relationships that could have appeared to influence the work reported in this paper.

References

[1] C. Artini, F. Locardi, M. Pani, I. Nelli, F. Caglieris, R. Masini, J.R. Plaisier, G.A. Costa, Yb-doped $Gd_2O_2CO_3$: structure, microstructure, thermal and magnetic behaviour, J. Phys. Chem. Solids 103 (2017) 59–66.
[2] Twinkle Mathew, R. Aishwarya Sree, S. Aishwarya, Khan Kounaina, Anirudh G. Patil, Pankaj Satapathy, S.P. Hudeda, Sunil S. More, K. Muthucheliyan, T. Naveen Kumar, Anjanapura V. Raghu, Kakarla Raghava Reddy, Farhan Zameer, FlatChem, 23 (2020) 100184.
[3] Yanyan Liu, Liangdong Fan, Yixiao Cai, Wei Zhang, Baoyuan Wang, Bin Zhu, Superionic Conductivity of Sm^{3+}, Pr^{3+}, and Nd^{3+} triple-doped ceria through bulk and surface two-step doping approach, ACS Appl. Mater. Interfaces 928 (2017) 23614–23623.
[4] S. Presto, C. Artini, M. Pani, M.M. Carnasciali, S. Massardo, M. Viviani, Ionic conductivity and local structural features in $Ce_{1-x}Sm_xO_{2-x/2}$, Phys. Chem. Chem. Phys. 20 (2018) 28338–28345.
[5] D Radhika, Karthik Kannan, A.S Neseraj, R Namitha, Facile low-temperature synthesis and application of La 0.85 Sr 0.15 Co 0.85 Fe 0.15 O 3-δ as superior cathode for LT-SOFCs using C-TAB as surfactant, Mater. Res. Innovat. 24 (7) (2020) 395–401.
[6] Yanyan Liu, Liangdong Fan, Yixiao Cai, et al., Superionic conductivity of Sm^{3+}, Pr^{3+} and Nd^{3+} triple-doped ceria through bulk and surface two-step doping approach, ACS Appl. Mater. Interfaces. 928 (2017) 23614–23623.
[7] Karthik Kannan, Devi Radhika, Kishor Kumar Sadasivuni, Kakarla Raghava Reddy, Anjanapura V. Raghu, Adv. Colloid Interface Sci. 281 (2020) 102178.
[8] K. Karthik, S. Dhanuskodi, S. Prabukumar, C. Gobinath, S. Sivaramakrishnan, Multifunctional properties of chemical precipitated CdO–NiO–ZnO mixed metal oxide nanocomposite: enhanced photocatalytic and antibacterial activities, J. Mater. Sci: Mater. Electron. 29 (2018) 5459–5471.
[9] S. Rana, J. Rawat, R.D.K. Misra, Anti-microbial active composite nanoparticles with magnetic core and photocatalytic shell: TiO2–NiFe2O4 biomaterial system, Acta Biomater. 1 (6) (2005) 691–703.
[10] C.V. Reddy, I.N. Reddy, V.V.N. Harish, K.R. Reddy, N.P. Shetti, J. Shim, T.M. Aminabhavi, Efficient removal of toxic organic dyes and photoelectrochemical properties of iron-doped zirconia nanoparticles, Chemosphere 239 (2020) 124766.
[11] A. Chauhan, V. Kataria, V.K. Garg, Green fabrication of ZnO nanoparticles using Eucalyptus spp. leaves extract and their application in wastewater remediation, Chemosphere 247 (2020) 125803.
[12] R. Aswini, S. Murugesan, K. Kannan, Bio-engineered TiO_2 nanoparticles using *Ledebouria revoluta* extract: larvicidal, histopathological, antibacterial and anticancer activity, Int. J. Environ. Anal. Chem. (2020), https://doi.org/10.1080/03067319.2020.1718668.
[13] Dibyajyoti Haldar, Prangan Duarah, Mihir Kumar Purkait, MOFs for the treatment of arsenic, fluoride and iron contaminated drinking water: a review, Chemosphere 251 (2020) 126388.
[14] C. Artini, RE-doped ceria systems and their performance as solid electrolytes: a puzzling tangle of structural issues at the average and local scale, Inorg. Chem. 57 (2018) 13047–13062.
[15] S. Thomas, M.P. Rayaroth, S. Menacherry, U.K. Aravind, C. Aravindakumar, Sonochemical degradation of benzenesulfonic acid in aqueous medium, Chemosphere 252 (2020) 126485.
[16] B.A. van Driel, P.J. Kooyman, K.J. van den Berg, A. Schmidt-Ott, J. Dik, A quick assessment of the photocatalytic activity of TiO_2 pigments — From lab to conservation studio!, Microchem. J. 126 (2016) 162–171.
[17] T. Linda, S. Muthupoongodi, X. Sahaya Shajan, S. Balakumar, Fabrication and characterization of chitosan templated CdO/NiO nano composite for dye degradation, Optik 127 (20) (2016) 8287–8293.
[18] S. Srinivasa Rao, Hierarchical nanospheres of NiCoS/NF for high-performance supercapacitors, Nano-Struct. Nano-Objects 19 (2019) 100366, https://doi.org/10.1016/j.nanoso.2019.100366.
[19] Devi Radhika, A. S. Nesaraj, Preparation and characterization of NiO based nano-ceramic composites as alternative anode materials for solid oxide fuel cells (SOFCs), Journal of Nanostructures, 2019 (In press).
[20] A. Arabaci, Synthesis and characterization of Pr/Gd co-doped ceria by using the citric acid–nitrate combustion method, Solid State Ion. 326 (2018) 69–76.
[21] G. Dell'Agli, L. Spiridigliozzi, M. Pansini, G. Accardo, S.P. Yoon, D. Frattini, Effect of the carbonate environment on morphology and sintering behaviour of variously co-doped (Ca, Sr, Er, Pr) Samarium-doped ceria in co-precipitation/hydrothermal synthesis, Ceram. Int. 44 (2018) 17935–17944.
[22] V. Dave, A. Gupta, P. Singh, C. Gupta, V. Sadhu, Kakarla Raghava Reddy, Synthesis and characterization of celecoxib loaded PEGylated liposome nanoparticles for biomedical applications, Nano-Structures & Nano-Objects 18 (2019) 100288.
[23] Y. Tao, J. Shao, J. Wang, et al., Morphology control of $Ce_{0.9}Gd_{0.1}O_{1.95}$ nano powder synthesized by sol-gel method using PVP as a surfactant, J. Alloy Compd. 484 (2009) 729.
[24] Devi Radhika, A. Samson Nesaraj, Low temperature chemical precipitation and characterization of ceria based ceramic composite oxide materials, J. Metals Mater. Miner. 23 (2013) 67.
[25] C. Artini, M.M. Carnasciali, M. Viviani, S. Presto, J.R. Plaisier, G.A. Costa, M. Pani, Structural properties of Sm-doped ceria electrolytes at the fuel cell operating temperatures, Solid State Ion. 315 (2018) 85–91.
[26] Devi Radhika, A. Samson Nesaraj, Preparation and characterization of doped ceria nanoparticles by chemical precipitation, Asian Journal of Research, Chemistry 4 (2011) 1.
[27] Ata Chitsaz, Marzieh Jalilpour, Mohammad Fathalilou, Effects of PVP and CTAB surfactants on the morphology of cerium oxide nanoparticles synthesized via co-precipitation method, Int. J. Mater. Res. 104 (2013) 511.
[28] A. Devi Radhika, Samson Nesaraj, Namitha., R cost effective synthesis of co-doped CeO_2 nano composite oxides using CTAB as surfactant: application for LT-SOFC as electrolyte, utopia of global, Education 3 (2017) 1.

[29] Subhashish Dey, Ganesh Chandra Dhal, Cerium catalysts applications in carbon monoxide oxidations, Mater. Sci. Energy Technol. 3 (2020) 6–24.
[30] Akhilesh Ugale, N. Thejo Kalyani, S.J. Dhoble, Investigations on RE(TTA)3tppo (RE = Eu/Sm/Eu0.5 Sm0.5) rare earth β-diketonate complexes for OLEDs and solid state lighting, Mater. Sci. Energy Technol. 3 (2020) 51–63.
[31] H. Shashidharagowda, Shridhar N. Mathad, Effect of incorporation of copper on structural properties of spinel nickel manganites by co-precipitation method, Mater. Sci. Energy Technol. 3 (2020) 201–208.
[32] O. Oloye, O. Eterigho-Ikelegbe, M.O. Daramola, Synthesis and evaluation of a nanocomposite hydroxy sodalite/ceramic (HS/ceramic) membrane for pre-combustion CO_2 capture: characterization and permeation test during CO2/H2 separation, Mater. Sci. Energy Technol. 3 (2020) 225–231.
[33] A. Senthamizhan, K. Sambathkumar, S. Nithiyanantham, Physico-chemical, structural, optical and NLO studies on pure and La3+ doped l-arginine acetate crystals, Mater. Sci. Energy Technol. 3 (2020) 282–288.
[34] Santosh J. Uke, Gajanan N. Chaudhari, B. Anjali, Satish P. Bodade, Mardikar, Morphology dependant electrochemical performance of hydrothermally synthesized NiCo2O4 nanomorphs, Mater. Sci. Energy Technol. 3 (2020) 289–298.
[35] Sunaina Patil, Hari Prasad Dasari, Effect of fuel and solvent on soot oxidation activity of ceria nanoparticles synthesized by solution combustion method, Mater. Sci. Energy Technol. 2 (3) (2019) 485–489.
[36] Devi Radhika, A. Samson Nesaraj, Chemical precipitation and characterization of multi-component perovskite oxide nanoparticles – Possible cathode materials for Low Temperature Solid Oxide Fuel Cell, Int. J. Nano Dimen. 5 (2014) 1.
[37] J. Jasmine Ketzial, Devi Radhika, A. Samson Nesaraj, Low temperature preparation and characteri zation of doped $BaCeO_3$ nanoparticles by chemical precipitation, Int. J. Ind. Chem. 4 (2013) 1.
[38] Z. Gao, L.V. Mogni, E.C. Miller, et al., A perspective on low temperature solid oxide fuel cells, Energy Environ. Sci. 9 (2016) 1602.
[39] B.C.H. Steele, Appraisal of CGO electrolytes for IT-SOFC operating at 500°C, Solid State Ionics 129 (2000) 95–110.
[40] Ana B. Muñoz-García, Daniel E. Bugaris, Michele Pavone, Jason P. Hodges, Ashfia Huq, Fanglin Chen, Hans-Conrad zur Loye, Emily A. Carter, Unveiling structure–property relationships in Sr 2 Fe 1.5 Mo 0.5 O $6-\delta$, an electrode material for symmetric solid oxide fuel cells, J. Am. Chem. Soc. 134 (15) (2012) 6826–6833.
[41] Shanwen Tao, John T.S. Irvine, Discovery and characterization of novel oxide anodes for solid oxide fuel cells, Chem. Record 4 (2) (2004) 83–95.
[42] A. Deepi, G. Srikesh, A. Samson Nesaraj, One pot reflux synthesis of reduced graphene oxide decorated with silver/cobalt oxide: a novel nano composite material for high capacitance applications, Ceram. Int. 44 (16) (2018) 20524–20530.
[43] M. Mogensen, S. Skaarup, Kinetic and geometric aspects of solid oxide fuel cell electrodes, Solid State Ionics 86–88 (1996) 1151–1160.
[44] Ujwala O. Bhagwat, Jerry J. Wu, Abdullah M. Asiri, Sambandam Anandan, Sonochemical synthesis of Mg-TiO 2 nanoparticles for persistent Congo red dye degradation, J. Photochem. Photobiol., A 346 (2017) 559–569.
[45] Wael A. Aboutaleb, Radwa A. El-Salamony, Effect of Fe_2O_3-CeO_2 nanocomposite synthesis method on the Congo red dye photodegradation under visible light irradiation, Mater. Chem. Phys. 236 (2019) 121724, https://doi.org/10.1016/j.matchemphys.2019.121724.
[46] Belgassim Boutra, Nuray Güy, Mahmut Özacar, Mohamed Trari, Magnetically separable $MnFe_2O_4$/TA/ZnO nanocomposites for photocatalytic degradation of Congo Red under visible light, J. Magn. Magn. Mater. 497 (2020) 165994, https://doi.org/10.1016/j.jmmm.2019.165994.
[47] Mehrnaz Babaei Shekardasht, Mohammad Hadi Givianrad, Parvin Gharbani, Zohreh Mirjafary, Ali Mehrizad, Preparation of a novel Z-scheme g-C_3N_4/RGO/$Bi_2Fe_4O_9$ nanophotocatalyst for degradation of Congo Red dye under visible light, Diam. Relat. Mater. 109 (2020) 108008, https://doi.org/10.1016/j.diamond.2020.108008.
[48] Azam Zamani, Mirabdullah Seyed Sadjadi, Alireza Mahjoub, Mohammad Yousef, Nazanin Farhadyar, Synthesis, characterization and investigation of photocatalytic activity of ZnMnO3/Fe3O4 nanocomposite for degradation of dye Congo red under visible light irradiation, Int J Ind Chem (2020) https://doi.org/10.1007/s40090-020-00215-z.
[49] J. Srivind, V.S. Nagarethinam, M. Suganya, S. Balamurugan, D. Prabha, A.R. Balu, Visible light irradiated photocatalytic performance of SnS_2-CdO nanocomposite against the degradation of rhodamine B (cationic) and congo red (anionic) dyes, Mater. Sci. Eng., B 255 (2020) 114530, https://doi.org/10.1016/j.mseb.2020.114530.
[50] Muhammad Yose Rizal, Rosari Saleh, Suhendro Purbo Prakoso, Ardiansyah Taufik, Shu Yin, Ultraviolet- and visible-light photocatalytic and sonophotocatalytic activities toward Congo red degradation using Ag/Mn_3O_4 nanocomposites, Mater. Sci. Semicond. Process. 121 (2021) 105371.
[51] Karthik Kannan, D. Radhika, Maria P. Nikolova, Kishor Kumar Sadasivuni & Namitha R (2020) Structural and functional properties of rare earth-based (NiO-CGO) nanocomposite produced by effective multiple doping approach via co-precipitation, Materials Technology, DOI: 10.1080/10667857.2020.1755555.
[52] Aswini Rangayasami, Karthik Kannan, Swetha Joshi, Murugesan Subban, Bioengineered silver nanoparticles using Elytraria acaulis (L.f.) Lindau leaf extract and its biological applications, Biocatal. Agric. Biotechnol. 27 (2020) 101690.
[53] Md Abdus Subhan, Tanzir Ahmed, Nizam Uddin, Abdul Kalam Azad, Kulsuma Begum, Synthesis, characterization, PL properties, photocatalytic and antibacterial activities of nano multi-metal oxide NiO·CeO2·ZnO, Spectrochim. Acta Part A Mol. Biomol. Spectrosc. 136 (2015) 824–831.
[54] Md Abdus Subhan, Nizam Uddin, Prosenjit Sarker, Hiroyasu Nakata, Ryuzi Makioka, Synthesis, characterization, low temperature solid state PL and photocatalytic activities of Ag_2O·CeO_2·ZnO nanocomposite, Spectrochim. Acta Part A Mol. Biomol. Spectrosc. 151 (2015) 56–63.